Dissipative Solitary Waves in Granular Crystals

R. Carretero-González,[1] D. Khatri,[2] Mason A. Porter,[3] P. G. Kevrekidis,[4] and C. Daraio[2,*]

[1]*Department of Mathematics and Statistics, San Diego State University, San Diego, California 92182-7720, USA*
[2]*Graduate Aeronautical Laboratories (GALCIT) and Department of Applied Physics, California Institute of Technology,
Pasadena, California 91125, USA*
[3]*Oxford Center for Industrial and Applied Mathematics, Mathematical Institute, University of Oxford, OX1 3LB, United Kingdom*
[4]*Department of Mathematics and Statistics, University of Massachusetts, Amherst, Massachusetts 01003-4515, USA*
(Received 12 August 2008; published 16 January 2009)

We provide a quantitative characterization of dissipative effects in one-dimensional granular crystals. We use the propagation of highly nonlinear solitary waves as a diagnostic tool and develop optimization schemes that allow one to compute the relevant exponents and prefactors of the dissipative terms in the equations of motion. We thereby propose a quantitatively accurate extension of the Hertzian model that encompasses dissipative effects via a discrete Laplacian of the velocities. Experiments and computations with steel, brass, and polytetrafluoroethylene reveal a *common* dissipation exponent with a material-dependent prefactor.

Introduction.—Since the advent of the famous Fermi-Pasta-Ulam model over 50 years ago, nonlinear oscillator chains have received a remarkable amount of attention in a wide range of physical settings [1]. Areas of intense theoretical and experimental interest over the past decade include (but are not limited to) DNA double-strand dynamics in biophysics [2], coupled waveguide arrays in nonlinear optics [3], breathing oscillations in micromechanical cantilever arrays [4], and Bose-Einstein condensation in optical lattices in atomic physics [5].

Within this general theme of interplay between nonlinearity and discreteness, one of the key subjects has been the study of 1D granular materials, which consist of chains of interacting particles that start from point contact with each other and deform elastically when compressed. In contrast to classically studied disordered granular media, highly packed granular lattices have negligible frictional and rotational dynamics, in favor of axial stress propagation [6,7]. The highly nonlinear dynamic response of such "crystals" has been the subject of considerable attention [6,8–23]. Additionally, granular crystals can be created from numerous material types and sizes, which makes their properties extremely tunable [8–10]. This flexibility is valuable not only for basic studies of the underlying physics but also in potential applications such as shock [24] and energy absorbing layers [13,18,20,21], sound focusing devices (tunable acoustic lenses and delay lines), actuators [25,26], sound absorption layers, and sound scramblers [11,12,23].

While the standard Hertzian force model has been used extensively in most dynamical investigations and is now textbook material [8,27], recent experimentally motivated investigations have illustrated the challenging need to include dissipation effects [24,28–30]. Dissipative terms related to friction [31], plasticity [32], viscoelasticity [33], and viscous drag [23,30] have been proposed to model

particle collisions [6,7,27]. However, none of these models captures both qualitatively and quantitatively the decay and wave shape of the highly nonlinear solitary waves observed experimentally. It is this important experimental and theoretical aspect of packed granular lattices that we aim to tackle in this Letter through the combination of modeling, numerical and physical experiments, and a detailed comparison thereof. Based on the earlier propositions of Refs. [6,7,24,30], we illustrate the prevalent nature of dissipation in the form of a discrete Laplacian in the velocities with *uniform* exponent and a material-dependent prefactor. The broad interest of our findings stems not only from their general nature for granular crystals of different materials but also from the significance of similar models in other fields, such as 1D lattice turbulence [34].

Experimental setup.—We assembled a monodisperse chain of N beads (here we report results for $N = 70$ but we performed experiments for up to $N = 188$ with similar results) of different materials (see Table I) with radius $R = 2.38$ mm in a horizontal setup [see Fig. 1(a)] arranged in a four-garolite rod stand. (To ensure contact between the particles, the guide was tilted at 4°.) To directly visualize the waves, we embedded calibrated piezosensors ($RC \sim 10^3$ μs, Piezo Systems, Inc; see Fig. 1(b) of Ref. [11])

TABLE I.   Material properties (mass m, elastic modulus E, and Poisson ratio ν) for stainless steel [35,36], PTFE [11,37,38], and brass [39]. The last two columns present our best estimates, together with their standard deviation, of the dissipation coefficients (α, γ).

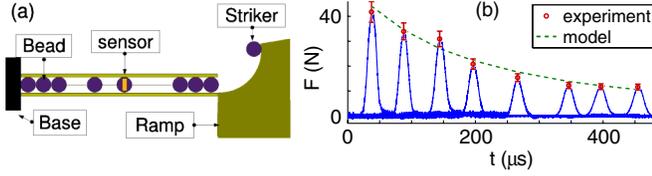| Material	m (g)	E (GPa)	ν	α	γ
Steel	0.45	193	0.30	1.81 ± 0.25	-5.58 ± 1.30
PTFE	0.123	1.46	0.46	1.68 ± 0.16	-1.56 ± 0.19
Brass	0.48	103	0.34	1.85 ± 0.13	-6.84 ± 0.66

FIG. 1 (color online). (a) Schematic diagram of the experimental setup. (b) Solitary wave decay in a chain composed of 70 steel particles impacted by a steel bead with $v_{\rm imp} = v_1$. The (blue) solid curves correspond to the recordings for sensors placed in particles 9, 16, 24, 31, 40, 50, 56, and 63.

inside selected particles, as described in Refs. [10–13]. We generated solitary waves by impacting the chain with a striker (identical to the particles in the chain) launched along a ramp. We calculated the impact velocities $v_{\rm imp}$ (in m/s) using a high-speed camera at the end of the ramp: $v_{1,2} = 1.77$, $v_{3,4} = 1.55$, $v_{5,6} = 1.40$, $v_{7,8} = 1.04$, and $v_{9,10} = 0.79$.

Model.—We model a dissipative chain of N spherical beads as a 1D lattice with Hertzian interactions [8]:

$$\ddot{y}_n = A(\delta_n^{3/2} - \delta_{n+1}^{3/2}) + \gamma s |\dot{\delta}_n - \dot{\delta}_{n+1}|^\alpha, \quad (1)$$

where $s \equiv {\rm sgn}(\dot{\delta}_n - \dot{\delta}_{n+1})$, $A \equiv E\sqrt{2R}/[3m(1 - \nu^2)]$, $n \in \{1, \ldots, N\}$, y_n is the deviation of the nth bead from its equilibrium, $\delta_n \equiv \max\{y_{n-1} - y_n, 0\}$ for $n \in \{2, \ldots, N\}$, $\delta_1 \equiv 0$, $\delta_{N+1} \equiv \max\{y_N, 0\}$, E is the Young's (elastic) modulus of the beads, ν is their Poisson ratio, m is their mass, and R is their radius. The particle $n = 0$ represents the striker. Dissipation is incorporated by using a phenomenological force with prefactor $\gamma < 0$, between adjacent beads that depends on their relative velocities (in particular, on the "discrete Laplacian" in the velocities), generalizing earlier models (with dissipation exponent $\alpha = 1$ specifically) for dry granular matter [30].

In contrast to previous works that *a priori* assume that $\alpha = 1$ (i.e., that model dissipation using a linear dashpot) [30], we determine both α and γ by directly comparing experimental and numerical results. The general coefficient α is thus a phenomenological parameter derived from the best fitting. We introduce the absolute value and the sign parameter s into (1) to ensure that genuine dissipation is guaranteed irrespective of the sign of the relative velocities between consecutive beads. The units of γ would depend on the value of α and, accordingly, are more properly investigated in dynamic models that incorporate dissipation based on detailed measurements of restitutive losses that cannot currently be achieved experimentally [6]. Importantly, the value we obtain for α differs decidedly from the coefficients used in previous modeling attempts [30] (see the discussion below).

Determining the dissipation coefficients.—We now determine the "optimal" dissipation coefficients (α, γ) from the experimental data for different materials and different configurations. The experimental data consist of the time series of the force through each sensor. We optimize the

pair (α, γ) by minimizing the following two differences between numerics and each particular experiment:

$$D(\alpha, \gamma) = \frac{1}{N} \sum_{n=1}^{N} \frac{|F_m^{\rm expt}(n) - F_m^{\rm num}(n)|}{\bar{F}_m^{\rm expt}}, \quad (2)$$

$$\Delta_n(\alpha, \gamma) = \frac{1}{T} \int_{t_i}^{t_f} \frac{|F^{\rm expt}(t; n) - F^{\rm num}(t; n)|}{\bar{F}^{\rm expt}(n)} dt, \quad (3)$$

where $\bar{F}_m^{\rm expt} \equiv (1/N) \sum_{n=1}^{N} F_m^{\rm expt}(n)$, $\bar{F}^{\rm expt}(n) = \int_{t_i}^{t_f} F^{\rm expt}(t; n) dt$, $F(t; n)$ is the time series data of the force through the nth sensor [see Fig. 1(b)], and $F_m(n) = \max_t\{F(t; n)\}$ is the maximum force recorded by the nth sensor over the recording time span $[t_i, t_f = t_i + T]$, where T is typically about 100 μs. The superscripts "expt" and "num" denote, respectively, the experimental and numerical data. The function $D(\alpha, \gamma)$ measures the "distance" between the numerics and the experiment using the *maxima* of the forces through all sensors of the experiment. The function $\Delta_n(\alpha, \gamma)$ measures the difference between experimental and numerical pulse shapes that go through the nth sensor. In order to avoid biasing $\Delta_n(\alpha, \gamma)$ with the difference in force magnitude [which is already taken into account when optimizing $D(\alpha, \gamma)$], we rescale the experimental data so that the numerical and experimental maxima match before we compare wave forms. That is, $F^{\rm expt}(t; n) \rightarrow F^{\rm expt}(t; n) F_m^{\rm num}(n)/F_m^{\rm expt}(n)$. Figures 2(a) and 2(b) depict, respectively, the differences $D(\alpha, \gamma)$ and $\Delta_n(\alpha, \gamma)$ in a particular (α, γ) range for a steel chain using a sensor placed towards the end of the chain. As can be observed from these panels, the optimization of the force maxima $F_m^{\rm num}$ [Fig. 2(a)] and the force pulse shape [Fig. 2(b)] are not sufficient on their own to determine the dissipation parameters. However, it is meaningful (and well defined) to optimize force maxima *and* pulse shape together by taking the intersection between the minima of each case (see the point at the intersection of the solid curves and dashed curves). For experiment j (with impact velocity v_j), we average the parameter pair (α_j, γ_j) over four sensors located throughout the bead chain. Finally, we average $(\alpha, \gamma) = \frac{1}{N_e} \sum_{j=1}^{N_e} (\alpha_j, \gamma_j)$ over the $N_e = 10$ different experiments to obtain the optimal dissipation parameters (α, γ) and compute the standard deviation for the N_e experiments.

We summarize our results, for three different set of experiments—using steel, Teflon [polytetrafluoroethylene (PTFE)], and brass beads—in the last two columns of Table I. In order to validate the results of the above optimization procedure *a posteriori*, we take the optimal dissipation parameters for the steel bead chain and compare the maximal forces obtained numerically with the experiments in Fig. 2(c). In Fig. 2(c), we show two typical examples (for impact velocities v_3 and v_8) and also plot the curves incorporating the standard deviation measured in our analysis. As can be clearly observed, all experimental data points fall well within the predicted region. To further
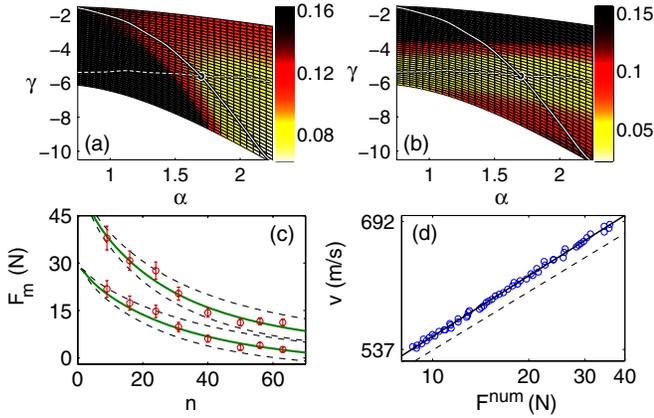
FIG. 2 (color online).   Optimization of the dissipation coeffi-
cients (α, γ) for a steel chain. (a) Difference $D(\alpha, \gamma)$, as defined
in Eq. (2), between the force maxima recorded in the experiment
and our model. (b) Difference $\Delta_n(\alpha, \gamma)$, as defined in Eq. (3), in
wave forms between the experiment and our model for sensor
$n = 56$. The solid curves and dashed curves correspond to the
minima obtained from (a) and (b), respectively. (c) Maximum
force $F_m^{\mathrm{num}}(n)$ for experiments with $v_{\mathrm{imp}} = v_3$ (top curves) and
$v_{\mathrm{imp}} = v_8$ (bottom curves, displaced by 5 units for clarity). The
(red) circles correspond to the experiment, and the (green) thick
curves give the numerical best fit with $(\alpha, \gamma) = (1.81 \pm
0.25, -5.58 \pm 1.30)$. The dashed curves correspond to the ex-
treme cases using the standard deviation found in the optimal
parameters. (d) Velocity of traveling front versus the maximum
force (in a log-log plot). The solid curve represents the best
linear fit, which gives $v \propto F_m^{0.17}$; we also show a dashed line with
slope 1/6.

validate our results, we compared the dependence of
the pulse velocity v against the maximal force F_m^{num} in
Fig. 2(d). This panel shows a typical example; we obtained
similar results (not shown here) for the other configura-
tions. The obtained exponent is extremely close to the
theoretical value of 1/6 (shown by the dashed line) [8].

In order to gain a deeper understanding of the role of the
dissipation exponent α, we depict in Fig. 3 the pulse shape
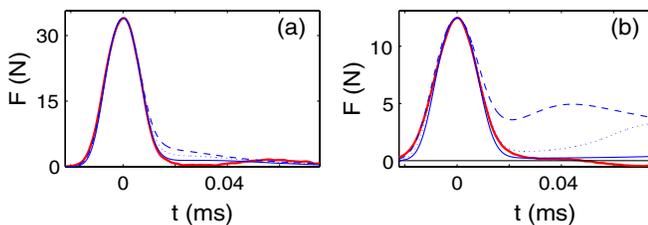for two sensors in the steel chain (one near the beginning of

FIG. 3 (color online).   Force versus time for the steel chain with
$v_{\mathrm{imp}} = v_2$ through sensors at positions (a) $n = 16$ and
(b) $n = 56$. The (red) thick solid curve depicts the (smoothed;
see text) experimental series, and the thin (blue) dashed curves,
dotted curves, and solid curves, respectively, show the numerics
with $(\alpha, \gamma) = (1, -5.5)$, $(1.4, -6)$, and $(1.81, -5.58)$. The last
case corresponds to the best fit (see text) for the dissipation
parameters for the chains of steel beads.

the chain and the other one near the end). We depict the
experimental pulse (smoothed by nearest-neighbor averag-
ing) with the (red) solid curve. The thin (blue) curves,
depict three numerical runs using three different pairs
(α, γ) along the minimum curve [shown by a solid curve
in Fig. 2(a)].

It is interesting to note that for all materials tested,
higher impact velocities correspond to a faster initial decay
as compared to the latter part of the chain (probably related
to the initiation of plasticity at the contact). Also, by
comparing the wave decay in chains composed of steel
and Teflon (or brass) beads, a faster and more pronounced
energy loss is evident for the softer beads. To understand
this dissipation physically, one should explore a more de-
tailed analysis of the contact plasticity, inelastic restitution,
and hydrodynamic drag.

Note that the optimal dissipation exponent α for the
three material types considered is consonant with a value
close to $\alpha = 1.75$. This indicates the *prevalence* of the
phenomenological damping introduced in Eq. (1), which is
one of the principal findings of this Letter. It is important to
point out the disparity of this optimal exponent from earlier
investigations, which focused on the (linear dashpot) case
of $\alpha = 1$ [24,30,34]. On the other hand, the dissipation
prefactor γ naturally does depend on the material. For steel
and brass, which have similar material properties, γ is also
similar (steel has $\gamma = -5.58$ and brass has $\gamma = -6.84$).
However, for Teflon, as can be anticipated from the much
lower elastic modulus E, the prefactor γ is significantly
smaller ($\gamma = -1.56$).

We show typical examples of the results for Teflon (left
column) and brass (right column) in Fig. 4. The top panels
depict the maximal force through the chain using the
optimal dissipation parameters. Note in the pulse shape
results (bottom panels) for Teflon and brass that low dis-
sipation exponents α tend to overestimate the size of the
secondary pulse hump. Another relevant observation, in
connection with its much smaller dissipation prefactor γ, is
that chains of Teflon beads may offer the first unambiguous
observation of the *secondary pulses* [see Fig. 4(c)] argued
in Ref. [30] to arise for weaker dissipation.

Conclusions.—In this Letter, we have offered for the first
time a quantitative and systematic modeling attempt at the
role of dissipation in granular crystals. Through detailed
comparison of numerical simulations and experiments in a
variety of materials (steel, Teflon, and brass), we have
demonstrated a generic functional form of the dissipation,
modeled by a phenomenological term based on the second
difference of the velocities between adjacent beads (i.e., a
discrete Laplacian) that is raised to a common exponent.
This allowed us to augment the standard dynamical model
based on Hertzian forces to encompass this dissipation
effect in (optimal) quantitative agreement with our experi-
ments. We found that the dissipation prefactor is material
dependent and that the considerably weaker prefactor of
Teflon (in comparison to brass and steel) allows one to
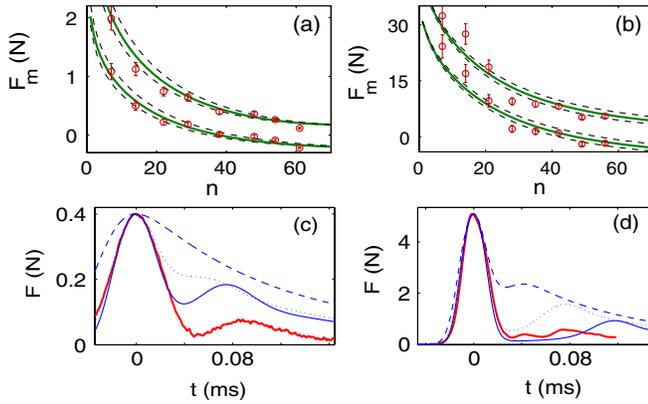observe unambiguously (and for the first time) secondary

FIG. 4 (color online).   Results for the Teflon (left column) and
brass (right column) experiments. The top panels depict the same
information as Fig. 2(c) for experiments with impact velocities
(a) v_3 (top curves) and v_8 (bottom curves, displaced by 0.3 units
for clarity) and (b) velocities v_3 (top curves) and v_6
(bottom curves, displaced by 7 units for clarity). The best fit
for the dissipation parameters for Teflon and brass are, respec-
tively, $(\alpha, \gamma) = (1.68 \pm 0.16, -1.56 \pm 0.19)$ and $(\alpha, \gamma) =$
$(1.85 \pm 0.13, -6.84 \pm 0.66)$. The bottom panels show the
same information as in Fig. 3. In (c), we depict the force versus
time through the sensor at $n = 38$ with $(\alpha, \gamma) = (1, -1.56)$,
$(1.4, -1.56)$, and $(1.68, -1.56)$. In (d), we show the same
information for the sensor at $n = 14$ with $(\alpha, \gamma) = (1, -5.5)$,
$(1.4, -6)$, and $(1.85, -6.84)$.

pulses such as the ones proposed in Ref. [30]. Our study
also provides a starting point for future quantitative inves-
tigations of this newly proposed model. For example, it
would be worth examining the critical prefactor below
which a secondary wave should be expected to emerge,
the interplay of the role of dissipation and plasticity (and a
quantitative incorporation of the latter) in the dynamics,
and extensions of the present considerations to higher-
dimensional settings.

---

*Corresponding author.
daraio@caltech.edu

[1] E. Fermi *et al.*, Los Alamos National Laboratory
Technical Report No. LA-1940, 1955; D. K. Campbell
et al., Chaos **15**, 015101 (2005).
[2] M. Peyrard, Nonlinearity **17**, R1 (2004).
[3] Y. S. Kivshar and G. P. Agrawal, *Optical Solitons: From
Fibers to Photonic Crystals* (Academic, San Diego, 2003).
[4] M. Sato, B. E. Hubbard, and A. J. Sievers, Rev. Mod. Phys.
78, 137 (2006).
[5] O. Morsch and M. Oberthaler, Rev. Mod. Phys. **78**, 179
(2006); V. A. Brazhnyi and V. V. Konotop, Mod. Phys.
Lett. B **18**, 627 (2004).
[6] S. Sen, J. Hong, J. Bang, E. Avalos, and R. Doney, Phys.
Rep. **462**, 21 (2008).
[7] H. M. Jaeger *et al.*, Rev. Mod. Phys. **68**, 1259 (1996).
[8] V. F. Nesterenko, *Dynamics of Heterogeneous Materials*
(Springer-Verlag, New York, 2001).
[9] C. Coste, E. Falcon, and S. Fauve, Phys. Rev. E**56**, 6104
(1997).
[10] C. Daraio, V. F. Nesterenko, E. B. Herbold, and S. Jin,
Phys. Rev. E **73**, 026610 (2006).
[11] C. Daraio, V. F. Nesterenko, E. B. Herbold, and S. Jin,
Phys. Rev. E **72**, 016603 (2005).
[12] V. F. Nesterenko, C. Daraio, E. B. Herbold, and S. Jin,
Phys. Rev. Lett. **95**, 158702 (2005).
[13] C. Daraio *et al.*, Phys. Rev. Lett. **96**, 058002 (2006).
[14] E. Hascoët and H. J. Herrmann, Eur. Phys. J. B **14**, 183
(2000).
[15] E. J. Hinch and S. Saint-Jean, Proc. R. Soc. A **455**, 3201
(1999).
[16] M. Manciu *et al.*, Physica (Amsterdam) **157D**, 226 (2001).
[17] J. Hong and A. Xu, Appl. Phys. Lett. **81**, 4868 (2002).
[18] J. Hong, Phys. Rev. Lett. **94**, 108001 (2005).
[19] S. Job and F. Melo, Phys. Rev. Lett. **94**, 178002 (2005).
[20] R. Doney and S. Sen, Phys. Rev. Lett. **97**, 155502 (2006).
[21] L. Vergara, Phys. Rev. E **73**, 066623 (2006).
[22] A. Sokolow *et al.*, Europhys. Lett. **77**, 24002 (2007).
[23] E. B. Herbold, V. F. Nesterenko, and C. Daraio, in *Shock
Compression of Condensed Matter*, AIP Conf. Proc.
No. 845 (AIP, New York, 2006), pp. 1523–1526.
[24] E. B. Herbold and V. F. Nesterenko, Phys. Rev. E **75**,
021304 (2007).
[25] D. Khatri, C. Daraio, and P. Rizzo, Proc. SPIE Int. Soc.
Opt. Eng. **6934**, 69340U (2008).
[26] C. Daraio and P. Rizzo, U.S. provisional patent application
filed 2008.
[27] K. L. Johnson, *Contact Mechanics* (Cambridge University
Press, Cambridge, England, 1985).
[28] N. V. Brilliantov, F. Spahn, J. M. Hertzsch, and T. Pöschel,
Phys. Rev. E **53**, 5382 (1996); S. McNamara and E.
Falcon, Phys. Rev. E **71**, 031302 (2005).
[29] C. Brunhuber, F. G. Mertens, and Y. Gaididei, Phys. Rev. E
73, 016614 (2006).
[30] A. Rosas, A. H. Romero, V. F. Nesterenko, and K.
Lindenberg, Phys. Rev. Lett. **98**, 164301 (2007).
[31] W. J. Wang and Z. G. Zhu, Europhys. Lett. **82**, 24004
(2008).
[32] I. Pane and E. Blank, Int. J. Solids Struct. **43**, 2014 (2006).
[33] W. A. M. Morgado and I. Oppenheim, Phys. Rev. E **55**,
1940 (1997).
[34] M. Peyrard and I. Daumont, Europhys. Lett. **59**, 834
(2002).
[35] *ASM Metals Reference Book* (American Society for
Metals, Metals Park, OH, 1983), 2nd ed.
[36] http://www.efunda.com.
[37] www.dupont.com/teflon/chemical/.
[38] W. J. Carter and S. P. Marsh, Los Alamos National
Laboratory Technical Report No. LA-13006-MS, 1995.
[39] http://www.matweb.com.